Optimizing the concentration ratio of multi-faceted focusing heliostats

Francois Henault, Gilles Flamant, Cyril Caliot

Optimizing the concentration ratio of multi-faceted focusing heliostats

François Hénault[a], Gilles Flamant[b], Cyril Caliot[c]

(a) Optical Engineering Consulting, 740 Chemin d'Argevillières, 07000 Veyras – France

(b) Processes, Materials and Solar Energy laboratory, PROMES CNRS, 7 Rue du Four Solaire, 66120 Font-Romeu-Odeillo-Via – France

(c) CNRS, UPPA, E2S, LMAP, 1 Allée du parc Montaury, 64600 Anglet – France

ABSTRACT

This paper aims at optimizing the concentration ratio of multi-faceted focusing heliostats implemented into a solar tower power plant. The ideal shape of a heliostat located off-axis in the field is known to be the local section of a fictitious paraboloïd whose parameters are varying continuously with the Sun angular position. We describe an optimization procedure applicable to those heliostats. The flux densities formed at the solar receiver and the achievable concentrating ratios are computed using an improved convolution algorithm. It is shown that the optimized heliostat shape can produce typical concentration gains of approximately 10%, even when the heliostats reflect the Sun under large incidence angles.

Keywords: Solar concentrator; Heliostat; Flux density; Concentration ratio; Optimization

1 INTRODUCTION

It is well known that the ideal shape of a focusing heliostat in a solar tower power plant is the local section of a fictitious paraboloïd whose focus is located at the centre of the solar receiver, and the optical axis is parallel to the Sun vector **S** at a given time [1-3]. Consequently, the ideal shape of the heliostat changes continuously with the time of the day and the day of the year. This drawback may be removed by defining a "Sun reference position" $\mathbf{S_0}$ from which the heliostat parameters are fixed. Such improvement only involves slight re-alignments of the tilt angles of the heliostat mirrors around the horizontal and vertical axes, so that they become tangent to the ideal paraboloïd shape. This paper describes an optimization procedure applicable to multi-faceted focusing heliostats (Section 2). The flux densities formed at the solar receiver and the achievable concentrating ratios are computed using an improved convolution algorithm (Section 3). It is shown that the optimized heliostat shape can produce gains of approximately 10% in terms of concentration ratio when compared with spherical heliostats. A brief conclusion is drawn in Section 4.

2 PRINCIPLE

2.1 Solar tower plant configuration

Let us consider the case of a solar tower power plant whose general configuration is depicted in Figure 1-A. Two main coordinate systems are defined:

- The X'Y'Z' reference frame attached to the solar receiver with X'-axis directed from South to North, Y'-axis from East to West, and Z'-axis from Nadir to Zenith,
- The OXYZ reference frame attached to an individual heliostat with centre O, where X is its optical axis and YZ are the lateral dimensions along which its geometry is defined (see Figures 1-B, 1-C and Table 1).
- Three vectors are defined in the X'Y'Z' reference frame (Figure 1-A):
  - **S** is a unit vector directed to the centre of the moving Sun,
  - **R** is the unit target vector directed from the heliostat centre to the solar receiver. It may be noted that this model can be applied to a cylindrical solar receiver illuminated from a North-South heliostat field without loss of generality.
  - **N** is the bisecting vector between both previous ones.

The vectors **S**, **R** and **N** obey the Snell-Descartes law for reflection that writes in vectorial form as:

$$\mathbf{S} + \mathbf{R} = 2(\mathbf{S}\,\mathbf{N})\,\mathbf{N} = 2\cos i\,\mathbf{N}, \tag{1}$$

with i the Sun incidence angle. The main employed parameters are summarized in Table 1. We consider the case of a heliostat located at coordinates (86.6, 50., 0.) expressed in meters into the X'Y'Z' reference frame with respect to the base of the tower. It may be noted that the distance d from the heliostat to the solar receiver is kept equal to 100 meters and that the heliostat and the solar receiver are located at the same altitude along the Z'-axis, which is considered as the worst and most demanding case. The heliostat is made of m x n identical spherical facets of focal length $f = d$ = 100 m. This is a simplified version of the focusing heliostats implemented at the solar tower power plant in Targasonne (France) located at 42° 30' 05'' North and 1° 58' 27'' East.

Table 1: Main parameters of the solar power plant and its focusing heliostat. The +sign designates heliostats located on the North side of the solar tower and the –sign those located on its South side.

Parameter	Symbol	Value	Unit
Height of solar receiver	h_R	86.6	m
Target vector from heliostat to receiver	**R**	(±86.6, 50., 0.)	m
Distance from heliostat to receiver	d	100	m
Incidence angle on solar receiver	β	30	degrees
Heliostat width along Y-axis	w	3.4	m
Heliostat height along Z-axis	h	3.	m
Number of heliostat facets	m x n	4 x 2	
Facet width along Y-axis	w_M	0.7	m
Facet height along Z-axis	h_M	1.4	m
Facet focal length	f	100	m
Solar receiver diameter	d'	1.2	m
Mean Sun angles in azimuth and height	(a_0, h_0)	(0., 44.63)	degrees
Mean Sun incidence angle (*)	i_0	25.98	degrees
Mean Sun incidence angle (**)	i_0	64.02	degrees

(*) North-side heliostat

(**) South-side heliostat

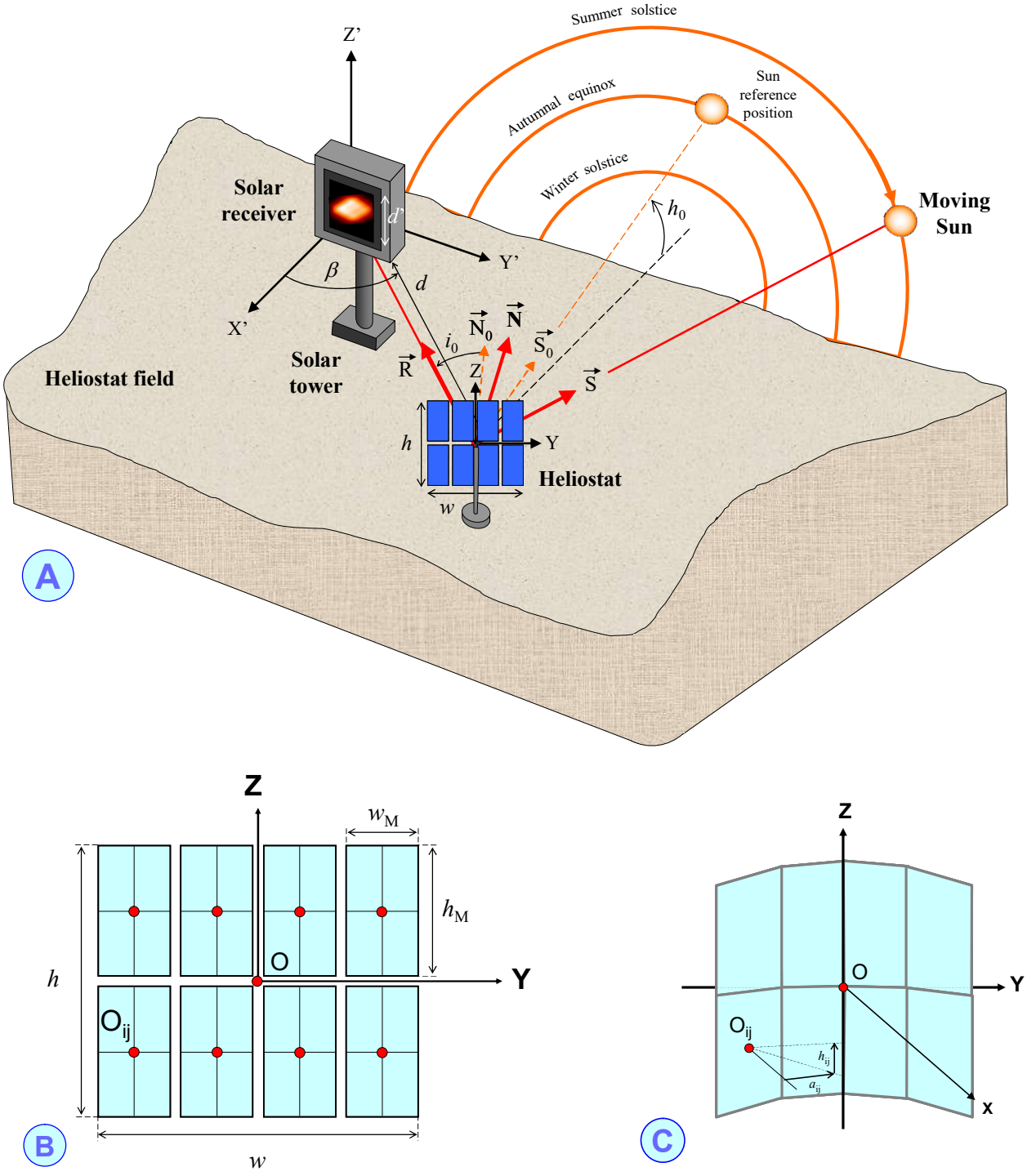

Figure 1: Solar tower power plant illuminated from a North heliostat field (A). The geometry of the heliostat (B) and its facets (C).

2.2 Heliostat canting strategies

Since their early development in the 70-80's years the solar tower power plants have been confronted with the problem of efficiently canting hundred or even thousands of focusing heliostats. A number of relevant studies have already been published [1-3], among which three main canting strategies emerged and are summarized as follows.

On-axis canting. This is the oldest and simple one where the heliostat facets approximate a spherical or a symmetric paraboloïd surface, both of them being equivalent in the usual case when the output numerical aperture of the heliostat is low enough. Such mirrors only produce sharp Sun images in the unrealistic case when the Sun vector **S**, the heliostat normal **N** and the target vector **R** are perfectly parallel. Otherwise, these heliostats are known to suffer from defocus and astigmatism aberrations considerably degrading the image quality under high incidence sunrays [4-6]. Practically speaking, their facets are generally adjusted by means of inclinometers such as described in Refs. [7-8].

Empirical off-axis canting. This strategy consists in selecting a Sun vector **S** differing from the target vector **R**, and optimizing the shape and the facet geometry of the mirror in order to maximizing its concentrating power at that particular position of the Sun [1-3]. The optimal shape of the mirror actually is the off-axis section of a paraboloïd determined from the triplet vector (**S**,**N**,**R**) as demonstrated by Igel and Hugues [9]. This means that the heliostat beam is perfectly focused at the solar receiver for a given off-axis Sun position. However this advantage exhibits two major drawbacks:

- Firstly, it has been demonstrated both theoretically and experimentally that the concentrating power of this heliostat rapidly falls down as long as the actual Sun vector **S** moves away from its preset value [1-3].
- Moreover, in the early years the heliostats were pointed at the chosen Sun position and their images were observed onto a target plane located near to the solar receiver. The facets were then manually adjusted in order to minimizing the beam size at the target. Since it usually takes a certain time to adjust one single heliostat while the Sun vector **S** still varies, the canting of the individual facets is affected with bias errors deteriorating the expected performance.

It finally turned out that this type of off-axis heliostats does not offer a significant performance gain with respect to the classical on-axis one.

Preset off-axis canting. This method differs from the previous one in the sense that a preset reference position $\mathbf{S_0}$ of the Sun vector is now directed at a mean position of the Sun during the time of day and for different days of the year (see Figure 1-A). The most intuitive choice is to hold the vector $\mathbf{S_0}$ at solar noon in the spring or autumn equinox days in order to balance the Sun variation angles throughout the year. Then all heliostats should achieve their maximum concentration at the same time. Obviously, this procedure requires using computer-aided inclinometers. Such specific canting strategy has been employed recently at the Sandia National Solar Thermal Test Facility [10] and is the baseline of the fore going study. Herein the method is also extended to heliostats located at the South side of the solar tower.

2.3 Optimal heliostat shape

Here it is assumed that all heliostat facets are identical. Then the sole degrees of freedom available for optimizing the off-axis heliostat are the tilt angles of each individual facet around the Y and Z axes. The employed optimization procedure is as follows:

1. We firstly define a "Sun reference position" that is assumed to be an averaged position all over the year. It is assumed to be reached at noon on the autumnal equinox day. It corresponds to the Sun reference vector $\mathbf{S_0}$ plotted in Figure 1.
2. The Sun vector $\mathbf{S_0}$ and target vector **R** are geometrically transferred from the X'Y'Z' reference frame to the OXYZ coordinate system.
3. Knowing both unitary vectors $\mathbf{S_0}$ and **R** enables determining the unitary vector $\mathbf{N_0}$ normal to the heliostat for that Sun position. By inversion of Eq. 1 it comes:

$$\mathbf{N_0} = \left(\mathbf{S_0} + \mathbf{R}\right) \Big/ \sqrt{2\left(1 + \mathbf{S_0}\mathbf{R}\right)}\,. \tag{2}$$

   Then the reference incidence angle on the heliostat is equal to $i_0 = \arccos(\mathbf{S_0}\mathbf{N_0})$.

4. From the knowledge of vectors $\mathbf{S_0}$, $\mathbf{N_0}$ and the incidence angle i_0; the tilt angles $a_{i,j}$ and $h_{i,j}$ of each heliostat facet are evaluated using a set of analytical formulas defined by Eqs. 3. These formulas are strictly equivalent to those presented in Ref. [9]. Alternatively, these angles could be determined with the help of standard ray-tracing software such as Zemax™.

$$a_{i,j} = \frac{y_{i,j}}{2d}\left(\frac{\cos^2 i_0 \cos^2\phi + \sin^2\phi}{\cos i_0}\right) - \frac{z_{i,j}}{4d}\frac{\sin 2\phi \sin^2 i_0}{\cos i_0}$$
$$h_{i,j} = -\frac{y_{i,j}}{4d}\frac{\sin 2\phi \sin^2 i_0}{\cos i_0} + \frac{z_{i,j}}{2d}\left(\frac{\cos^2 i_0 \sin^2\phi + \cos^2\phi}{\cos i_0}\right) \quad (3)$$

where $y_{i,j}$ and $z_{i,j}$ are the coordinates of each facet centre and $\phi = \arctan(s_{0Y}, s_{0Z})$ with (s_{0Y}, s_{0Z}) the direction cosines of the reference Sun vector $\mathbf{S_0}$ along the Y and Z axes. All of them are expressed into the local heliostat reference frame XYZ.

3 NUMERICAL RESULTS

After a short introduction about the employed numerical models (§ 3.1) this section presents the main numerical results obtained for heliostats located at the North side of the solar tower (§ 3.2) and then at its South side (§ 3.3).

3.1 Numerical models

The flux density maps formed by the different heliostats at the receiver plane Y'Z' are computed from a double Fast Fourier Transform (FFT) convolution algorithm. Cross-checking its results with those obtained using a Grid ray-tracing (GRT) model leads to RMS error differences lower than 1% [11]. Here two different heliostat canting strategies are distinguished:

A. Case of one single heliostat located at the coordinates (±86.6, 50., 0.) expressed in meters into the X'Y'Z' reference frame,

B. Case of a couple of heliostats being symmetric with respect to the X'-axis and located respectively at the coordinates (±86.6, 50., 0.) and (±86.6, -50., 0.) meters into the X'Y'Z' reference frame. Then the flux density maps formed by each heliostat are simply added one to the other. The case B is the most commonly encountered since the heliostat fields generally present a symmetry with respect to the X'-axis.

The angular radiance law of the Sun often named as "sunshape" may be the subject of many choices, especially between the most recent ones describing the circumsolar radiation [12-14]. However, they involve some atmospheric parameters that may not change the canting strategies significantly. Hence was selected the classical Jose's formula [15] giving a fair representation of the Sun's limb darkening effect, and writing as:

$$R(\varepsilon) \approx R_0\left(0.39 + 0.61\sqrt{1-(\varepsilon/\varepsilon_0)^2}\right), \quad (4)$$

where ε_0 is the angular radius of the Sun, ε the deviation angle with respect to its centre, and R_0 a normalizing factor typically equal to 1.47 10^7 W/m2/sr in clear sky conditions at ground level.

3.2 Northern heliostats

This is the most encountered case since heliostats located at the North side of a solar tower experience lower incidence angles of the sunrays when compared with Southern heliostats, thus minimizing astigmatism aberrations. In this example, the preset angle i_0 of the Sun is about 26 degrees (see Table 1). The values of the optimized angles $a_{i,j}$ and $h_{i,j}$

are given in Table 2 for each heliostat facet, and compared with those of the spherical heliostat. The flux densities formed at the solar receiver are computed using the FFT convolution algorithm for both the spherical and off-axis heliostat cases. They are illustrated by false-colour maps in Figure 2.

The achieved concentrating ratios by the spherical and off-axis heliostats are presented in Table 3 for both cases A (x 1) and B (x 2) that are illustrated in Figure 3. They show a net advantage of about 10 % in terms of concentrating power for the off-axis heliostats. It must be noted that this gain occurs around half time of the day, typically from 10h00 to 14h00 GMT, while it drops to ≈ 3 % over the full day.

Table 2: Tilt angles of the spherical and off-axis heliostat facets and their differences in terms of milli-radians. North heliostat case.

	Spherical heliostat		**Off-axis heliostat**		**Angles difference**		
Indices i, j	Tilt wrt Z $a_{i,j}$	Tilt wrt Y $h_{i,j}$	Tilt wrt Z $a_{i,j}$	Tilt wrt Y $h_{i,j}$	Tilt wrt Z $a_{i,j}$	Tilt wrt Y $h_{i,j}$	Unit
1, 1	12.75	7.50	14.19	8.34	1.44	0.84	mrad
2, 1	4.25	7.50	5.20	7.55	0.95	0.05	mrad
3, 1	-4.25	7.50	-3.85	6.78	0.40	-0.72	mrad
4, 1	-12.75	7.50	-12.94	6.04	-0.19	-1.46	mrad
1, 2	12.75	-7.50	12.75	-5.89	0.00	1.61	mrad
2, 2	4.25	-7.50	3.80	-6.70	-0.45	0.80	mrad
3, 2	-4.25	-7.50	-5.19	-7.49	-0.94	0.01	mrad
4, 2	-12.75	-7.50	-14.24	-8.24	-1.49	-0.74	mrad

Table 3: Achieved concentration ratios by both the spherical and off-axis heliostats (top and bottom rows respectively). Cases of a single North heliostat (x 1) and of two of them being symmetric with respect to the X'-axis (x 2).

	09-23-2022, Day time GMT				
Concentration ratio	T = 09h00	T = 10h30	T = 12h00	T = 13h30	T = 15h00
Spherical heliostat (x 1)	38.1	37.7	32.9	16.4	6.5
Spherical heliostat (x 2)	44.6	54.1	65.9	54.1	44.6
Off-axis heliostat (x 1)	32.0	35.7	35.7	24.3	6.5
Off-axis heliostat (x 2)	38.5	60.0	71.4	60.0	38.5

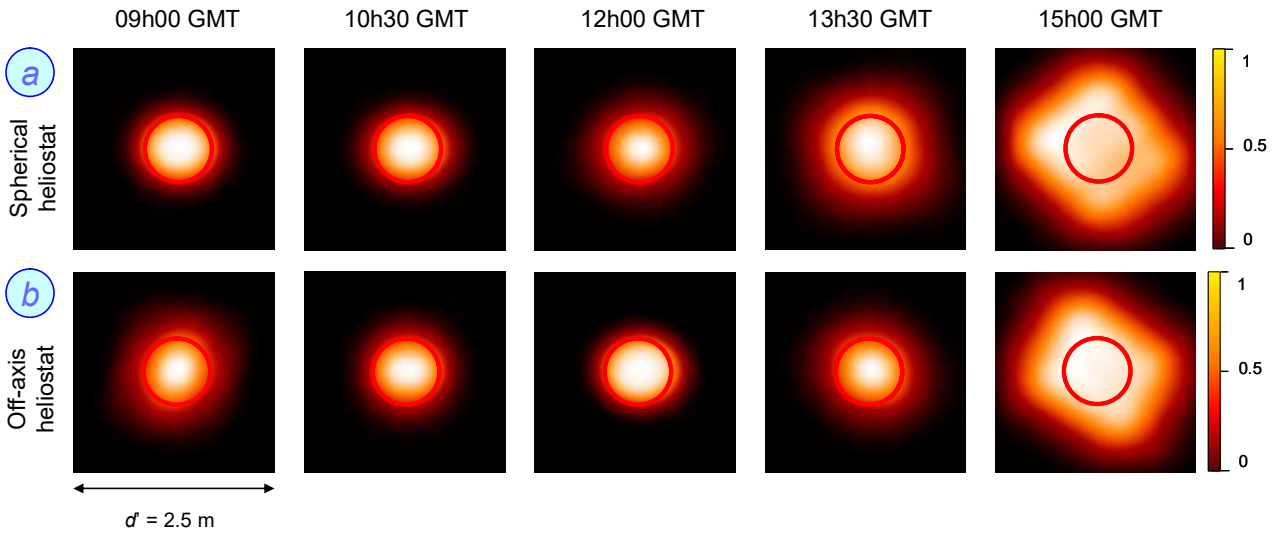

Figure 2: Flux densities formed at the solar receiver by North heliostats. (*a*) Case of spherical heliostat. (*b*) Case of the optimized off-axis heliostat. Red circles indicate the diameter of the ideally focused Sun image.

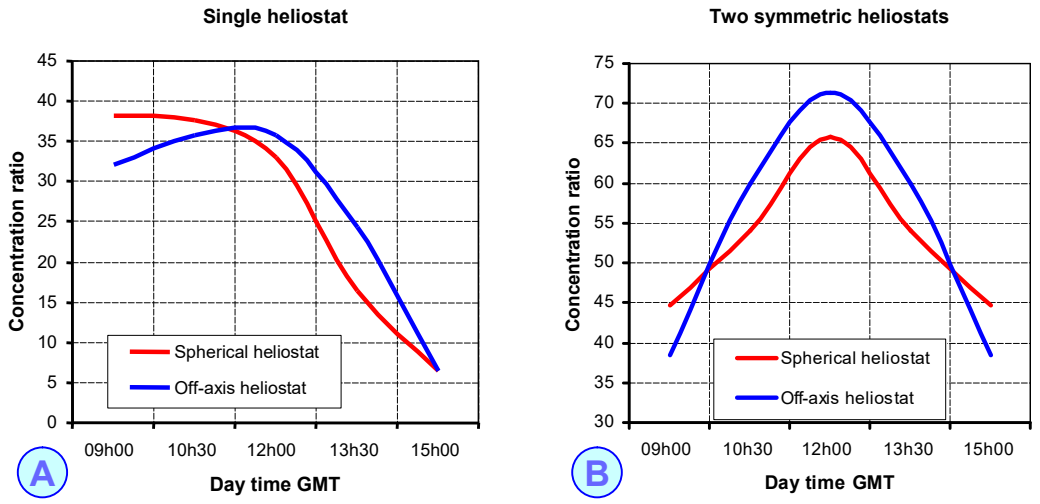

Figure 3: Achieved concentration ratios by both North spherical and off-axis heliostats. (A) Case of one single heliostat. (B) Case of two symmetric heliostats with respect to the X'-axis.

3.3 Southern heliostats

It is also of interest to check the efficiency of the off-axis strategy for heliostats located at the South side of the solar tower. Here is considered a similar couple of heliostats as in the previous subsection, where the signs of the X' coordinates and the angles $a_{i,j}$ and $h_{i,j}$ of the spherical heliostat have been inverted (i.e. the system is fully symmetric with respect to the X'-axis). In such case, the preset angle i_0 of the Sun can be as high as 64 degrees. The same presentations as in the previous subsection are shown. The values of the optimized angles $a_{i,j}$ and $h_{i,j}$ are given in Table 4 for each facet, and compared with those of the spherical heliostat. The flux densities formed at the solar receiver are illustrated by false-colour maps in Figure 4. The achieved concentrating ratios by the spherical and off-axis heliostats are given in Table 5 and illustrated in Figure 5.

Assuming the same distance d = |OO'| from the heliostat to the centre of the solar receiver, it is found that the Sun images are now fully dominated by a dramatic astigmatism aberration, especially for what concerns the on-axis heliostat. This is illustrated by the target width d' that had to be multiplied by a factor about 8 in Figure 5. It follows that its concentration ratio is always lower than unity all along the day. Better results are obtained using the off-axis canting strategy that achieves peak and mean values of 2.5 and 1.7 respectively, which correspond to relative concentrating gains of approximately 600 and 380 %. Thus the off-axis canting strategy looks even more efficient for Southern heliostats than for Northern ones. One may note however that such low concentrating powers may be improved by reducing the distance d from the heliostat to the centre of the solar receiver, because the astigmatism effect is know to be proportional to that distance. For example, setting d = 10 m instead of 100 m would roughly improve the concentration by a factor of 10. Other significant gains will also be achieved when installing the solar power plant at lower geographical latitudes, and raising the height of the solar tower. Hence a global optimization of these parameters and of a possible asymmetric distribution of the heliostat field would be required. Such studies have already been published elsewhere (see e.g. [16-18]) but are beyond the scope of the present paper.

Table 4: Tilt angles of the spherical and off-axis heliostat facets and their differences in terms of milli-radians. South heliostat case.

	Spherical heliostat		**Off-axis heliostat**		**Angles difference**		
Indices i, j	Tilt wrt Z $a_{i,j}$	Tilt wrt Y $h_{i,j}$	Tilt wrt Z $a_{i,j}$	Tilt wrt Y $h_{i,j}$	Tilt wrt Z $a_{i,j}$	Tilt wrt Y $h_{i,j}$	Unit
1, 1	-12.75	-7.50	22.16	22.94	34.91	30.44	mrad
2, 1	-4.25	-7.50	11.99	15.18	16.24	22.68	mrad
3, 1	4.25	-7.50	1.63	7.38	-2.62	14.88	mrad
4, 1	12.75	-7.50	-8.92	-0.44	-21.67	7.06	mrad
1, 2	-12.75	7.50	8.69	0.43	21.44	-7.07	mrad
2, 2	-4.25	7.50	-1.63	-7.26	2.62	-14.76	mrad
3, 2	4.25	7.50	-12.13	-14.98	-16.38	-22.48	mrad
4, 2	12.75	7.50	-22.82	-22.72	-35.57	-30.22	mrad

Table 5: Achieved concentration ratios by both the spherical and off-axis heliostats (top and bottom rows respectively). Cases of a single South heliostat (x 1) and of two of them being symmetric with respect to the X'-axis (x 2).

	09-23-2022, Day time GMT				
Concentration ratio	T = 09h00	T = 10h30	T = 12h00	T = 13h30	T = 15h00
Spherical heliostat (x 1)	0.20	0.18	0.17	0.15	0.16
Spherical heliostat (x 2)	0.36	0.33	0.33	0.33	0.36
Off-axis heliostat (x 1)	0.92	1.17	1.27	0.30	0.26
Off-axis heliostat (x 2)	1.17	1.47	2.53	1.47	1.17

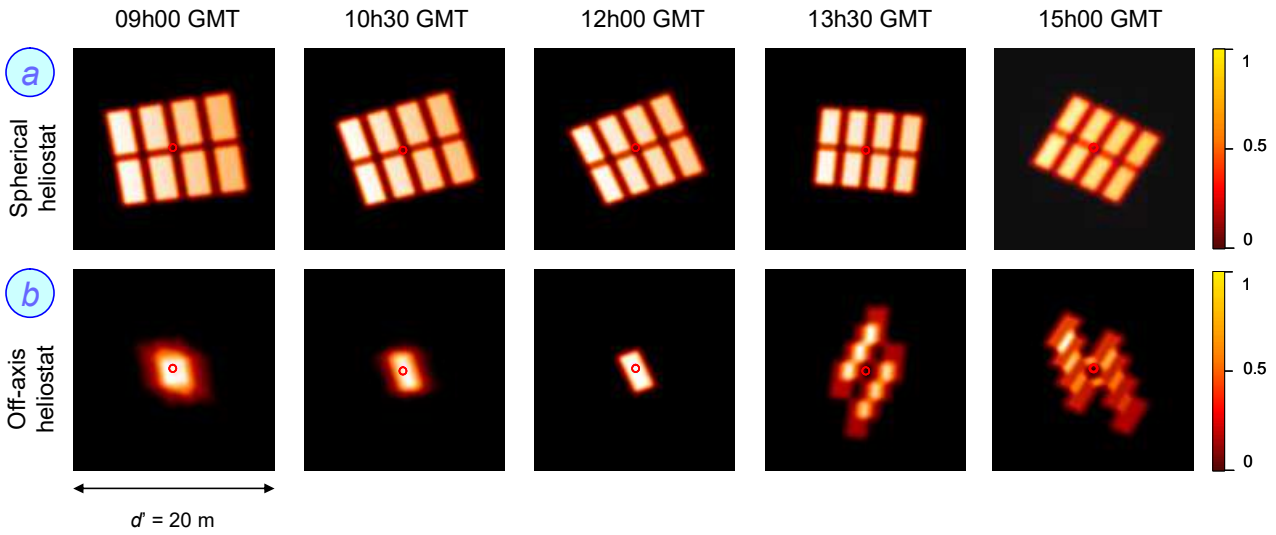

Figure 4: Flux densities formed at the solar receiver by South heliostats. (*a*) Case of spherical heliostat. (*b*) Case of the optimized off-axis heliostat. Red circles indicate the diameter of the ideally focused Sun image.

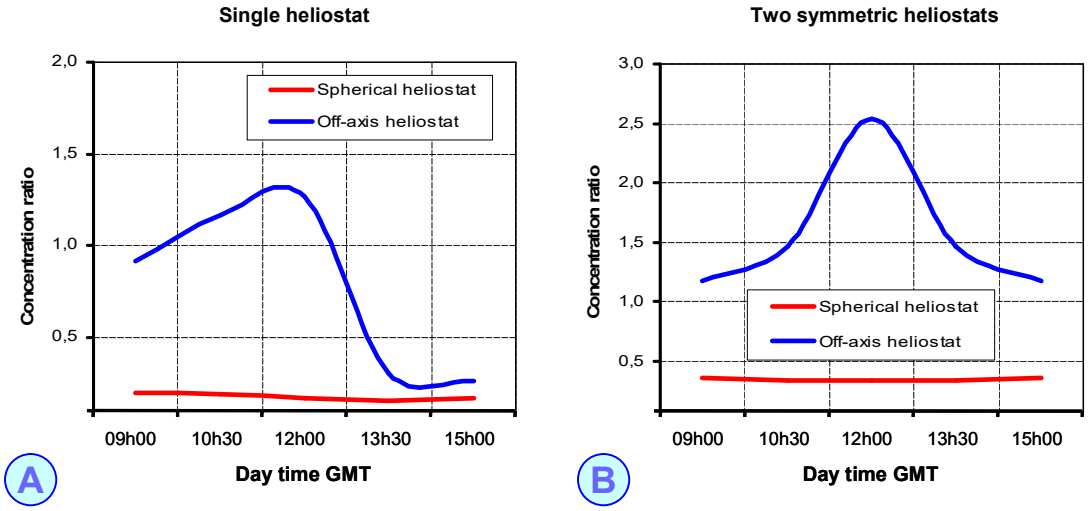

Figure 5: Achieved concentration ratios by both the spherical and off-axis South heliostats. (A) Case of one single heliostat. (B) Case of two symmetric heliostats with respect to the X'-axis.

4 CONCLUSION

This contribution considers the case of a multi-faceted heliostat focusing sunrays at the central receiver of a solar tower power plant. It presents a solution to improve the concentrating ratio of the heliostat in Sun-tracking mode all over daytime operation. The optimization process consists in turning the shape of a classical spherical heliostat into an off-axis shape profile. Assuming that all heliostat facets are identical, the available degrees of freedom for optimizing the spherical heliostat are the tilt angles of each of its individual facets. The optimization procedure firstly defines a Sun reference position in the sky, then slightly modifies these angles so that they are become tangent to an ideal parabolic

section. A Fourier transform convolution model is used to evaluate the irradiance maps at the solar receiver and the achieved concentration ratios. Such an "off-axis" solution enables increasing the concentrating ratio of the heliostats by about 10 %. This procedure may be extended to the entire heliostat field, provided that the individual facet inclinations $a_{i,j}$. and $h_{i,j}$ are pre-defined by software to feed a versatile mechanical adjustment tool such as inclinometers [7-8]. Thus the concentration power at the solar receiver could be maximized. This would be especially valuable for test facilities whose main purpose is to achieve a highest solar flux at the moment of a test near solar noon.

REFERENCES

1. S. A. Jones, "Recent Results on the Optical Performance of Solar Two Heliostats," Sandia National laboratories Report SAND94-2776C (1994).
2. S. A. Jones, "A Comparison of On-Axis and Off-Axis Heliostat Alignment Strategies," Sandia National laboratories Report SAND96-0566C (1996).
3. R. Buck, E. Tuefel, "Comparison and Optimization of Heliostat Canting Methods," Journal of Solar Energy Engineering vol. 131 (2009).
4. W. Landman, P. Gauche, "Influence of canting mechanism and facet profile on heliostat field performance," Energy Procedia vol. 49, p. 126-135 (2014).
5. F. Hénault, "Fast computation of solar concentrating ratio in presence of opto-mechanical errors," Solar Energy vol. 112, p. 183-193 (2015).
6. A. Sanchez-Gonzalez, "Analytic function for heliostat flux mapping with astigmatism and defocus," Solar Energy vol. 241, p. 24-38 (2022).
7. J. Yellowhair, C. Ho, "Heliostat Canting and Focusing Methods: An Overview and Comparison. Proceedings of the 4th International Conference on Energy Sustainability (2010).
8. E. Sproul, K. Chavez, J. Yellowhair, "The Development of the Heliostat Focusing and Canting Enhancement Technique: An Optical Heliostat Alignment Tool for the National Solar Thermal Test Facility," Proceedings of the ASME 2011 5th International Conference on Energy Sustainability (2011).
9. E. Igel, R. Hugues, "Optical analysis of solar facility heliostats," Solar Energy vol. 22, p. 283-295 (1979).
10. R. C. Brost, A. Evans, T. Larkin, "Variation in Reflected Beam Shape and Pointing Accuracy Over Time and Heliostat Field Position," SolarPaces 2023 Conference Proceedings (2024).
11. F. Hénault, G. Flamant, C. Caliot, "Fast and accurate Computation of Flux Density formed by Solar Concentrators and Heliostats," Solar Paces conference 2023.
12. J. Noring, D. Grether, A. Hunt, "Circumsolar Radiation Data: The Lawrence Berkeley Laboratory Reduced Database," NREL Technical Report NREL/TP 262-4429 (1991).
13. A. Neumann *et. al*., "Representative Terrestrial Solar Brightness Profiles," Transactions of the ASME vol. 124, p. 198-204 (2002).
14. D. Buie, A. Monger, C. Dey, "Sunshape distributions for terrestrial solar simulations," Solar Energy vol. 74, p. 113-122 (2003).
15. P. Jose, "The flux through the focal spot of a solar furnace," Solar Energy vol. 1, p. 19-22 (1957).
16. M. Zhang, L. Yang, C. Xu, X. Du, "An efficient code to optimize the heliostat field and comparisons between the biomimetic spiral and staggered layout," Renewable Energy vol. 87, p. 720-730 (2016).
17. C. Li, R. Zhai, Y. Yang; "Optimization of a Heliostat Field Layout on Annual Basis Using a Hybrid Algorithm Combining Particle Swarm Optimization Algorithm and Genetic Algorithm," Energies vol. 10, n° 1924 (2017).
18. F. J. Collado, J. Guallar, "Quick design of regular heliostat fields for commercial solar tower power plants," Energy vol. 178, p. 115-125 (2019).